Transport in polycrystalline polymer thin-film transistors

R. A. Street,* J. E. Northrup, and A. Salleo
Palo Alto Research Center, 3333 Coyote Hill Road, Palo Alto, California 94304, USA
(Received 8 November 2004; revised manuscript received 17 December 2004; published 5 April 2005)

We describe a transport model for ordered polymer semiconductors that considers the physical and electronic structure, including the effects of hole delocalization in ordered lamella, grain boundary structures, a two-dimensional density of states, and percolation effects related to transport dimensionality. Simple model calculations are compared to experiments on regioregular polythiophene.

DOI: 10.1103/PhysRevB.71.165202 PACS number(s): 71.20.Rv, 72.80.Le, 82.35.Cd, 85.30.Tv

I. INTRODUCTION

Over the past decade or so the room-temperature mobility of polymer thin-film transistors has increased from about 10^{-5} to 0.1 cm^2/Vs,[1–5] with organic small molecules having a mobility of up to $1-5$ cm^2/Vs and single crystals even higher.[6] The dominant cause of the increase is the improvement in structural order, and such a relation between order and mobility is expected for any disordered material. Previous transport models of low-mobility amorphous (or mostly amorphous) polymer semiconductors make no specific assumptions about the polymer structure, which is implicitly taken to be isotropic and disordered.[7–9] A hopping model is usually applied to a broad Gaussian tail of localized states, and it is assumed that there are no accessible bandlike states. Instead, the dominant transport path is determined by a competition between an increasing density of localized states which favors a high hopping rate and the decreasing occupancy of the states. This model is able to account for a wide range of data on amorphous conducting polymers.

However, the high-mobility semiconducting polymers are far from being random structures.[10,11] Careful control over deposition and substrate surface preparation results in partially crystalline lamella layers that are highly oriented in the out-of-plane direction. The π-π stacking of the polymer rings allows hole delocalization between chains, giving two-dimensional transport within a lamella, rather than one-dimensional transport along a chain.[3,10] The polycrystalline structure also favors bandlike transport over hopping. Hence there is every reason to suppose that both the electronic structure and the transport mechanism are likely to be different from the amorphous polymers. Models of bandlike transport at a mobility edge, with a band tail of localized states that traps carriers have been successful in several high-mobility organic semiconductors such as pentacene and some polymers.[12–15]

The aim of this paper is to develop the transport model for high mobility polymers, taking into account the ordered structure. Our focus is on polymers for thin-film transistors (TFTs), and specifically poly(3-alkylthiophene)s (PAT) of which there are many variants.[10] A key aspect of transport in a polycrystalline polymer is the relative contribution of the grain and grain boundary material. Although a great deal is known about the lamella structure of ordered PAT,[10] the long-range structure is not known in detail. However, it seems useful to identify some key issues and general principles and see how much progress can be made in developing a structural model that can form the basis of a transport model that is capable of interpreting experimental results. The paper therefore first discusses the structure for the particular case of regioregular PAT, which so far has the highest mobility reported for a polymer. We then try to construct an appropriate density-of-states model along with transport mechanisms that allows a calculation of the conduction in a TFT and comparison with data.

Transport data

The conduction, σ, or mobility, μ, of polymers and polycrystalline organic small molecules usually approximate to a thermally activated behavior of the form,

$$\sigma = \sigma_0 \exp[E_F/kT]; \quad \mu = \mu_0 \exp[E_T/kT]. \tag{1}$$

Many measurements of transport in ordered organic semiconductors observe a change in the activation energy in the $100-250$ K temperature range, with the lower temperature region having a smaller activation energy and also a smaller prefactor.[14,16–18] However, in general, amorphous polymers and polycrystalline organic small molecules, such as pentacene,[19] often do not show a change of slope (see Fig. 2), although a gradual change reflecting hopping is sometimes observed. Our own measurements of regioregular poly(3,3‴-didodecylquarterthiophene) (PQT-12),[5] in Figs. 1–3, show transfer characteristics and the mobility as a function of temperature, and they are described in more detail elsewhere.[5,14,20] Transfer data in Fig. 1 show the subthreshold region usually observed in disordered materials. The subthreshold region becomes more extended at low temperatures.

Figure 2 shows the pronounced change in mobility activation energy at about 250 K. Below this temperature the energy is about 50 meV, depending on gate voltage, while at higher temperature the energy increases to 0.25 eV. However, there is no change of slope in material that has increased disorder, as shown in Fig. 2. One of the purposes of this paper is to try to understand the change in activation energy, particularly as this feature cannot be readily explained by simple transport models.

Extracting the temperature dependence of TFT parameters such as mobility from the transfer data is nontrivial, because the curvature in the TFT characteristics deviate from the

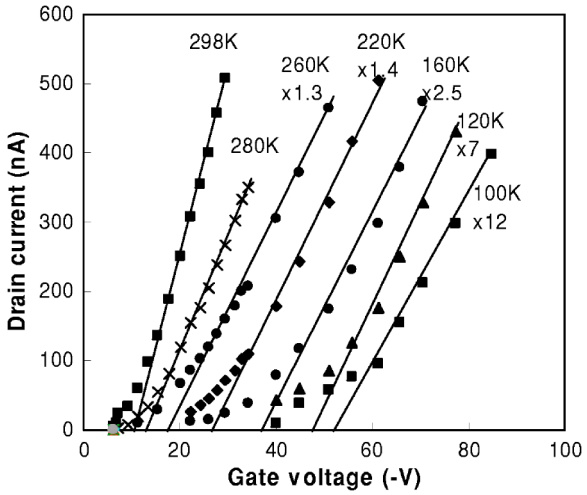

FIG. 1. Transfer characteristics of PQT-12 at different temperatures showing the increase in the threshold voltage. The data are measured with a pulsed gate voltage to reduce bias-stress effects and with a drain voltage of 1 V. The data are scaled by the factors indicated.

standard expressions.[12] The apparent threshold voltage increases at low temperature, and the apparent mobility depends on the choice of threshold voltage and gate voltage. The threshold voltage of polymer TFTs is generally several volts at 300 K and much larger at low temperature, and it reflects the trapping of immobile charges in localized states. The resulting measure of TFT mobility is a value for the mobile carriers, since the immobile carriers are automatically excluded from consideration. In a situation where there may be alternative transport mechanisms, a description of the effective mobility of all the carriers has less ambiguity, although it is certainly dependent on gate voltage. We therefore use two alternative descriptions of the mobility—the conventional μ_{TFT}, based on a fit to the TFT transfer data,

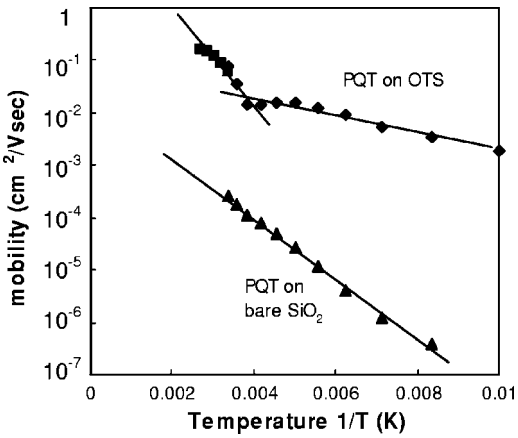

FIG. 2. TFT mobility vs inverse temperature for two samples of PQT-12, showing the change of activation energy near 250 K in the higher-mobility material, but not in the lower-mobility material. The high-mobility sample is deposited on an octadecyltrichlorosilane (OTS) self-assembled monolayer and the lower-mobility sample is the same material deposited on the untreated silicon oxide dielectric.

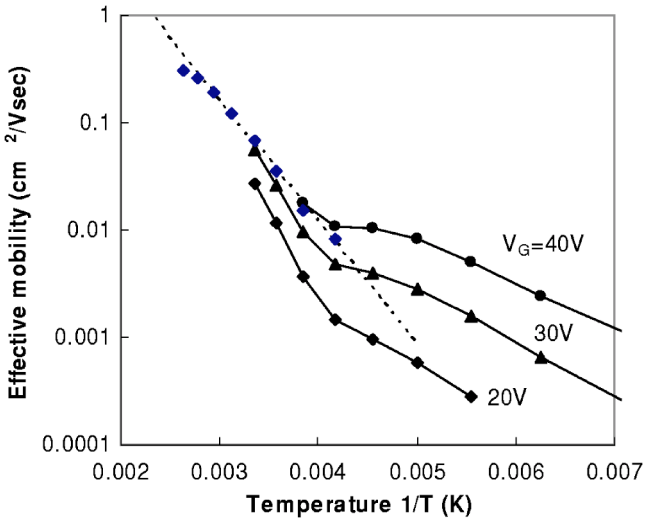

FIG. 3. Effective mobility (as defined in the text) vs inverse temperature for high-mobility PQT-12, measured at different gate voltages. The dashed line corresponds to an activation energy of 0.22 eV and a mobility prefactor of 500 $cm^2/V\,s$. The change of slope at the highest temperature, also seen in Fig. 2, is due to thermal changes in the sample.

and an effective mobility, μ_{EFF}, obtained by setting $V_T=0$, and applying the good approximation that the onset voltage, V_{ON}, is close to zero,

$$\mu_{EFF}(V_G) = \frac{I_{SD}}{C_G(V_G - V_{ON})}\frac{L}{W} \approx \frac{I_{SD}}{C_G V_G}\frac{L}{W} \qquad (2)$$

Figure 3 shows data for μ_{EFF} at different gate voltages. The data are similar to Fig. 2, with the change of slope at ~250 K, although the quantitative values differ. At low temperature, $\mu_{EFF} < \mu_{TFT}$ because of the threshold voltage effect, while above 250 K, the two values are similar, provided that the measurement is performed at high-enough V_G. The high temperature region from 250 to 400 K shows activation energy of 0.22 eV and the extrapolation to $1/T=0$ (the mobility prefactor) is 500 cm^2/Vs. It is tempting to associate the prefactor with a bulk mobility, but generally it also includes a large entropy factor, as we discuss in Sec. V A.

A previous model of transport in these TFTs has focused on the low-temperature region, and has shown that a band-tail model with isotropic conduction gives a reasonable description of the transport.[14] This paper looks at the transport in more detail to see if a more realistic model can account for the additional complexities of the higher-temperature data.

II. STRUCTURAL BASIS FOR A TRANSPORT MODEL

A. Polythiophene structure

High mobility PAT TFTs are made by the solution processing of regioregular material on a flat, hydrophobic surface, which promotes structural ordering.[3,5,10,21,22] The ordered PAT has a lamella structure formed of polymer chains which lie in the plane of the substrate, with the conjugated

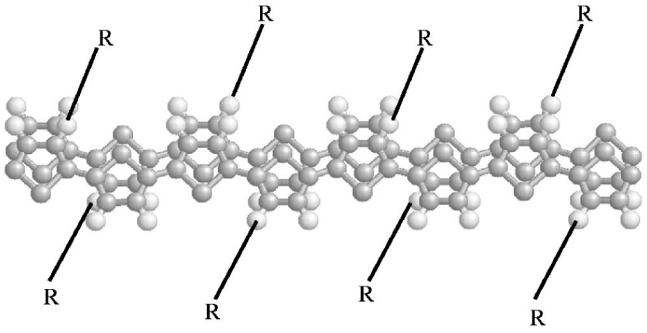

FIG. 4. Illustration of the structure of PQT-12 showing the ordering of the adjacent chains and the location of the alkyl chains, *R*. In PQT-12, $R=C_{12}H_{25}$, while in the model structure employed in the electronic structure calculation, *R* is represented by a single H atom. The registration between the chains is such as to minimize the interaction between the alkyl side chains with neighboring chains.

rings approximately perpendicular to the substrate, as illustrated in Fig. 4. The lamella planes are widely spaced (1.7 nm in PQT,[5] 1.2–3.0 nm in other PAT variants[10]), due to the long alkyl chains attached to the backbone.

Structural studies, including x-ray and atomic force microscopy (AFM), show that the ordered PAT lamella are nanocrystalline, and that the size of the ordered region is of order 10 nm. Sirringhaus reports 9.5 nm for poly(3hexyethiophene) (P3HT) from the x-ray measurement.[3] AFM measurements of PQT-12 show structures extending ~10 nm along the chain direction, stacking together into larger clusters.[23] There is a similar ordering of P3HT on graphite, except that the lamella are perpendicular to the substrate, so that the individual planes can be seen by AFM.[24] The average crystallite sizes are ~20 nm, and there are substantial regions of disordered material. Other growth conditions give a more needlelike microstructure.[25]

Figure 5 illustrates the generally accepted structure for an ordered nanocrystalline lamella. Within a nanocrystal region the chains are stacked side-by-side with considerable long-range order. At each end the polymer chains extend from the ordered region by differing amounts. This must occur because there is a distribution of chain lengths, but it probably would also occur in monodispersed material. The chain ends are presumed to contribute to the disordered material at the grain boundaries. The crystallite grains are not expected to be perfectly ordered because of the torsional rotations of the rings and the presence of chain ends, as well other possible chain defects and impurities. We should therefore anticipate a localized band tail within each grain, but expect that the disorder is less than in the intergranular regions.

Although highly textured in the vertical direction, the nanocrystals are randomly oriented in the *x-y* plane, since there is no preferred direction, at least for a dimension much larger than the grain size and in the absence of an alignment layer.[26,27] Individual lamella are therefore separated by grain boundaries, which we expect to have a more disordered structure. The transport model needs to explicitly include the grain boundary structure.

The accumulation-layer width of a TFT is typically about 1 nm, and since the lamella are separated by a larger distance, TFT transport is dominated by a single lamella plane. Therefore, to a good approximation, planes further from the dielectric interface do not need to be considered for the TFT transport model. This structure implies that a two-dimensional density of states should be used to model the transport, at least for the ordered regions. Transport in a single plane is probably one reason why the TFT mobility is very sensitive to the surface preparation of the gate dielectric.

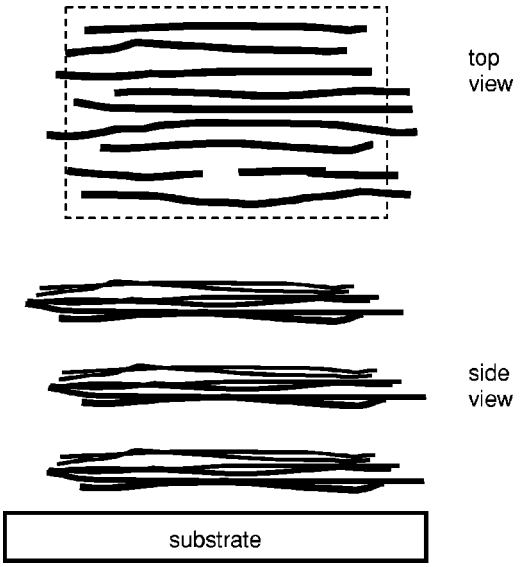

FIG. 5. Illustration of polythiophene lamella showing long-range order within the lamella, small local fluctuations in chain position, and disordered chain ends (adapted from Ref. 10). The alkyl chains are omitted.

B. Grain boundaries

The nanocrystalline lamella have very specific structural orientations in the plane, this being defined by the directions of their chains (see Fig. 5). The orientation implies that the electronic property of the boundary between two adjacent grains depends primarily on their relative orientations. Figure 6 illustrates small angle grain boundaries for lamella that are connected end-to-end with respect to the chain orientation. It seems natural to expect that the end-to-end structure will exhibit some interpenetration of the chains along with considerable disorder in the boundary. Side-to-side grains also have the possibility of a reasonably smooth connection at some locations. In either case the links between grains are bent chains of low bend angles. The significance for the transport is that we expect localized states to be associated with bent chains and with a correlation between the localization energy and the bend angle.

High-angle grain boundaries, also illustrated in Fig. 6, are more disordered. At the very least, the boundary is characterized by bent chains with a higher bend angle. Our conclusion is that grain boundaries are not isotropic, and that there are favorable and unfavorable transport directions across the boundaries, with the most favorable direction being where the angle is smallest.

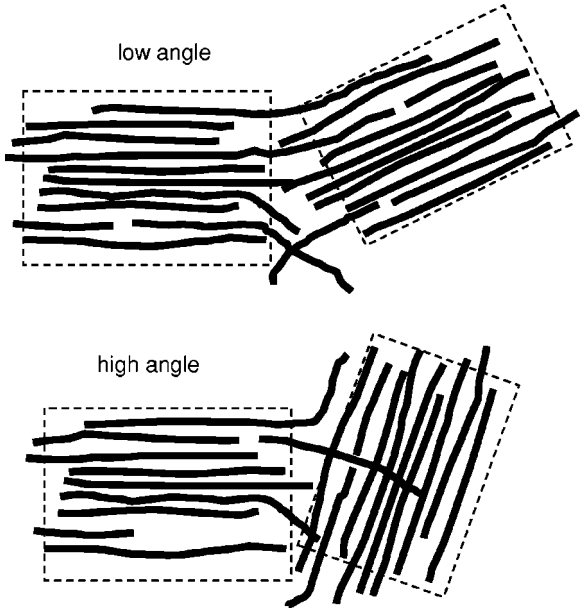

FIG. 6. Schematic illustration of possible grain boundary structure for small-angle (upper figure) and large-angle boundaries (lower figure), illustrating that the large-angle boundary has more disorder.

Disordered regions between grains are apparent in most AFM images of the structure, and it seems reasonable to expect that these regions are made up of amorphous material. A rough estimate of the ratio, F, of the area of the grain boundary layer to the area of the lamella, is,

$$F = 2d/L, \tag{3}$$

where L is the size of a crystallite and d is the width of the disordered region. Setting $L=20$ nm and $d=0.5-1.0$ nm gives $F=0.05-0.10$, so that 5–10% of the material is in the boundary, and d can hardly be less than 0.5 nm, because this is about the size of a single thiophene ring. Electronic states in the grain boundaries therefore cannot be ignored.

III. THE ELECTRONIC STRUCTURE

There have been many calculations of the electronic structure of polymers, mostly based on tight-binding calculations of single chains and typically focusing on single chains. To obtain a better understanding of the electronic structure of the ordered polymers, calculations of the ideal crystalline structure are performed to learn more about hole delocalization.

A. First principles calculations for PQT-12

The calculations of the atomic and electronic structure[28] for crystalline polythiophene use first-principles pseudopotentials[29] and density-functional theory.[30] A similar approach has been employed to calculate the structural properties of pentacene.[31,32] The two-dimensional sheets of polythiophene considered here are intended to represent the structure of regioregular, ordered PQT-12 films.[5] Calculations of

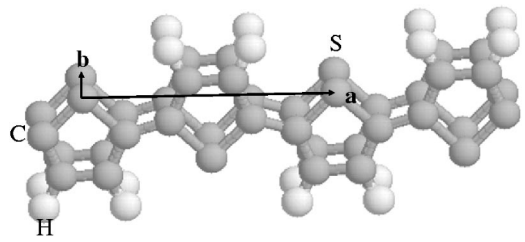

FIG. 7. Illustration of eight rings of an infinite two-dimensional sheet of polythiophene, as used for the electronic structure calculations. The smallest unit cell is described by the lattice vectors **a** and **b**, and the lengths of these vectors are determined by energy minimization. The lattice points $\mathbf{R}=n\mathbf{a}+m\mathbf{b}$ span a two-dimensional plane and the polythiophene material therefore forms a two-dimensional sheet. The calculations take place in a supercell with a third lattice vector **c** (length 14.8 Å) that is orthogonal to both **a** and **b**.

the equilibrium atomic structure for these sheets are performed, employing a unit cell containing eight C atoms, two S atoms, and four H atoms, as shown in Fig. 7. This cell is repeated in two dimensions with lattice vectors $\mathbf{a}=(a,0,0)$ and $\mathbf{b}=(0,b,0)$ to form an infinite sheet in the x-y plane. For calculational convenience periodicity is also assumed to exist in a third dimension with $\mathbf{c}=(0,0,c)$. The length of c is chosen to be sufficiently large to eliminate interactions between neighboring sheets in the **c** direction. Such chains are sufficiently long to eliminate interaction between sheets, so that the material is effectively two dimensional. These fully saturated side chains are electronically inert and are not included explicitly in this study. Electron-phonon interactions are not included in the calculation.

The wave functions are expanded in plane waves having kinetic energies up to 40 Ry. The two-dimensional Brillouin zone is sampled using 12 k points. The lattice vector **a**, which describes translations along the chains, was determined by energy minimization to have a length of 14.6 bohr, i.e., 7.7 Å. In addition to the internal coordinates of the polymer two other structural degrees of freedom are optimized: the distance between neighboring polythiophene chains and the angle of rotation of each chain along an axis running along the chains. The angle of rotation about the chain axis is determined to be 30° and the optimum spacing between chains is 7.2 bohr, i.e., 3.8 Å. The energy of the structure is reduced by 0.09 eV/(thiophene ring) by this rotation. While it is possible that the presence of alkyl side chains could lead to a different optimal chain rotation, this energy seems large enough to allow us to predict that a significant rotation of the polythiophene chains will be present—especially for polymers having a low density of side chains, such as PQT-12.

The electronic structure is calculated as a function of the interchain spacing and the results are shown in Fig. 8. The interaction between adjacent rings increases the bandwidth as the ring spacing decreases, and is associated with hole delocalization. At the equilibrium interchain spacing the hole bandwidth corresponding to the dispersion perpendicular to the chains is 0.60 eV. The corresponding bandwidth for the electrons is 0.19 eV. These values are obtained directly from the Kohn-Sham eigenvalue spectrum. A more accurate treat-

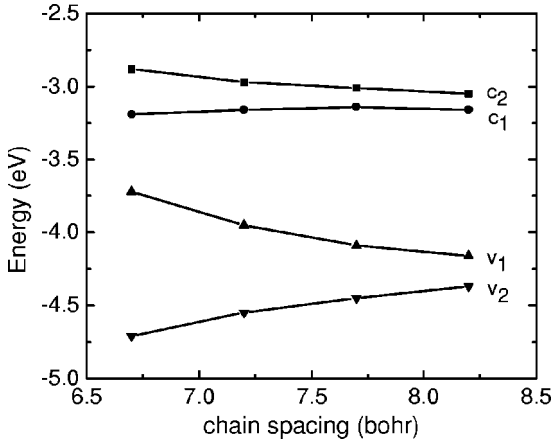

FIG. 8. The energy position, relative to the vacuum level, and the widths of the electron and hole bands, calculated as a function of the spacing between the chains. The energies v_1 and v_2 (c_2 and c_1) are the energies of the top and bottom of the hole (electron) band corresponding to transport perpendicular to the polymer chains.

ment, with a proper calculation of the electron self-energy, is likely to change these values by $\sim$20%.[32] It is clear from these results, nevertheless, that the matrix element for transfer from chain to chain is a factor of 3 larger for the valence band than for the conduction band. The greater bandwidth exhibited by the valence band is consistent with the fact that it is more sensitive to the interchain distance than the conduction band, as is apparent from Fig. 8. Consequently the valence-band edge will be more affected by structural order than the conduction-band edge.

The band structure is calculated for the equilibrium structure and the results are shown in Fig. 9. For both the electrons and the holes the dispersion along the chains (Γ-J) is much larger than the dispersion perpendicular to the chains (Γ-J$'$). The two-dimensional density of states is given approximately by $(2/\pi \mathrm{A})(W_1 W_2)^{-1/2} \sim 2\times 10^{14}/(\mathrm{eV\ cm}^2)$,

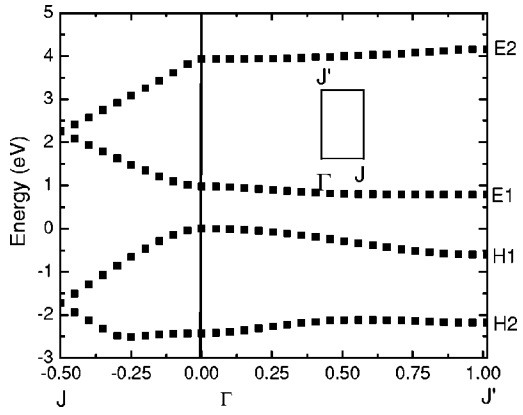

FIG. 9. Band structure for the two-dimensional sheet of PQT-12 for the lattice constants, $a=14.6$ bohr and $b=7.2$ bohr. The dispersion from Γ to $\mathrm{J}=(\pi/a,0)$ and from Γ to $\mathrm{J}'=(0,\pi/b)$ is shown. The topmost hole band $H1$ has a dispersion of 1.72 eV along Γ-J and a dispersion of 0.60 eV along Γ-J$'$. The zero of energy is at the valence-band maximum.

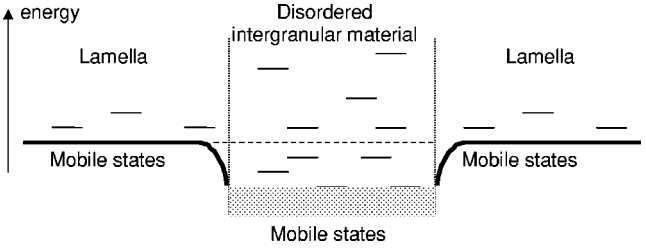

FIG. 10. Illustration of how the valence bands of ordered lamella and disordered intergranular regions of the valence band line up to give a barrier to holes transferring between lamella.

where W_1 and W_2 are the widths of the $H1$ band parallel and perpendicular to the chains (see Fig. 9) and A is the area of the two-dimensional unit cell.

The available experimental data are consistent with the calculations. Evidence for the hole delocalization is very clear from the optical absorption which shows that the band gap is reduced significantly in the ordered material. Brown *et al.* report a shift of about 0.5 eV in the optical absorption peak of P3HT and a broader band than in the regiorandom material.[33] Other measurements find a similar result, with a shift of about 0.3 eV at the onset of absorption between random and regular P3HT.[34] Photoluminescence in the same regioregular P3HT is shifted down by about 0.25 eV, which is consistent with the optical absorption.[34] A sharper optical-absorption edge correlates with increased mobility in PQT-12 optical absorption, and also the photoluminescence peak is close to the absorption edge, with a small Stokes shift.[5]

The agreed origin of these effects is that order-induced carrier delocalization increases the valence and conduction bandwidths and hence reduces the band gap. The calculations confirm the reduction of the gap and find that about $\frac{3}{4}$ of the shift occurs in the valence band, which suggests that the valence-band shift is about 0.3–0.4 eV between ordered and amorphous material.

B. Electronic structure of grain boundaries

The complete electronic structure of the polycrystalline material must take into account the difference between the ordered material making up the lamella and the disordered material in the grain boundaries. We consider the case of two ordered lamella with disordered material in between. According to our analysis of the electronic structure, Fig. 10 illustrates that two effects influence the alignment of states of the ordered and disordered material near the valence-band edge. The disordered region has a wider band tail of localized states because of the increased disorder, but the band is shifted down in energy compared to the ordered regions because of the hole delocalization.

The ordered regions therefore contain an energy barrier to the transport of the holes into the disordered regions because of the different energies of the band edges. Near the edge of a lamella the hole delocalization decreases and the band gap increases. Hence the band edge bends at the edge of the lamella in a way that confines holes in the lamella. The edge of an ordered lamella may have traps because of increased

disorder, but there is also a barrier limiting access to even deeper traps.

C. The density-of-states distribution

The electronic structure allows us to develop a density-of-states (DOS) distribution that can be used as the basis for a transport model. The DOS combines a two-dimensional density of states for the ordered lamella structure with the proposed shifted density of states for the disordered material between grains, and this is illustrated in Fig. 11. The two-dimensional (2D) DOS is constant in energy, in contrast to the square root energy dependence of a three-dimensional (3D) DOS. Hence, we assume that the lamella has a constant DOS above the gap and a narrow tail of localized states extending into the gap. The disordered grain boundary material has a much broader band tail, but the whole DOS is shifted into the valence band.

The TFT characteristics provide a rough estimate of the density of the traps. The voltage difference between the turn on, V_{ON}, and the threshold, V_T, is typically 5–10 V at 300 K, which corresponds to $\sim 10^{12}$ states/cm^2, lying deep enough (e.g., >0.2 eV) to prevent the Fermi energy from approaching the band edge. Since we expect that essentially all of the charge is contained within one lamella plane, this density of traps corresponds to about four traps for every 20×20 nm lamella. Considering our estimate that 5–10% of the material is in the disordered grain boundaries, the density of localized states seems small, and we suggest that it is evidence for the shifted-band-edge model, in which a substantial number of the localized states are pushed above the valence-band edge of the lamella.

D. Polarons

The presence of polarons is an important consideration for the electronic structure, because they are known to occur in amorphous polymers.[33–35] However, detailed measurements of photoinduced absorption (PA) show that the polaron energies are very different in disordered and ordered P3HT. There is a large polaron energy for regiorandom P3HT (the $P1$ PA band at 0.6 eV) but only a small energy for the regioregular P3HT (the $DP1$ PA band <0.1 eV).[33] This reduction in energy is also attributable to hole delocalization, because the polaron energy is sensitive to the localization of the wave function.

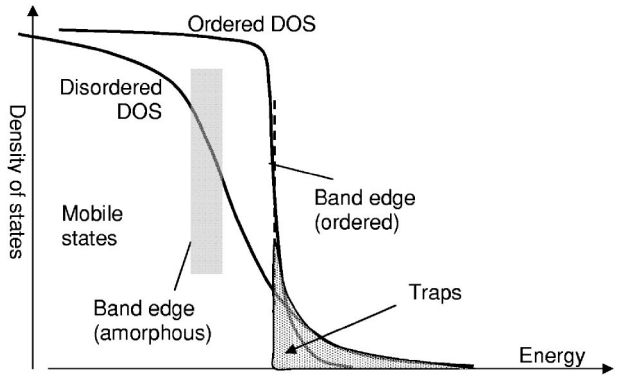

FIG. 11. Proposed density-of-states distribution combining ordered and disordered material and showing the sharp band edge and constant 2D DOS in the ordered layer and the shifted band edge, with a wider band tail for the disordered intergranular material.

In a simple polaron model the peak optical absorption of the polaron is twice the binding energy, W_P, while the hopping energy, W_H, is half the binding energy.[36] Hence the $P1$ measurements imply energies of $W_P=0.3$ eV, $W_H=0.15$ eV for disordered material and $W_P<0.05$ eV, $W_H<0.02$ eV for the ordered material. This means that polarons should be a large factor in the mobility and temperature dependence of transport in amorphous material. Polarons are less important in the ordered structures, but are still expected to cause a significant increase in the effective mass and a corresponding reduction of the band mobility.

Both the band-gap shift and the different polaron energies affect the electronic transport and must be taken into account in any detailed transport model. A key question regards the relative energies of the valence-band states in ordered and disordered material and the related relative energies of the transport paths. This question is complicated by several competing effects. We take the band edge of ordered PAT as the reference energy, E_0, for the DOS and the transport energy. Transport in disordered material occurs at energy

$$E_{TD} = E_0 + \Delta_{EG} - \Delta_{EP} - \Delta_{ED} \sim E_0 + 0.3 - 0.3 - \Delta_{ED}, \quad (4)$$

where Δ_{EG} is the band-edge shift due to hole delocalization (estimated above to be ~ 0.3 eV), Δ_{EP} is the difference in the polaron energy (also ~ 0.3 eV, as discussed above), and Δ_{ED} is the extra disorder energy of localized states. Energy is defined to be positive going into the valence band. The hole localization and the polaron energies therefore approximately offset each other.

Since the transport energy contains terms of opposite signs, it is not obvious that the disordered material has a transport path further into the band gap, compared to the ordered material, even though this is the natural expectation. The offset between the ordered and disordered materials due to hole localization is an important effect that may dominate the transport properties, and Sec. IV develops this theme.

IV. TRANSPORT MECHANISMS

The transport process involves conduction within the ordered nanocrystals, transfer across grain boundaries, and the long-range connectivity of the structure.

A. Transport within an ordered lamella

In our view, the appropriate model for transport within an ordered lamella is band transport, with a reasonably well-defined band edge and a narrow, localized state distribution. We think that a hopping model most likely applies to amorphous polymers, but that the nanocrystalline structure of high-mobility polythiophene makes the difference. The crystallites should be characterized by a band edge at which transport takes place, and which is similar from grain to grain. (Even though the lamella are small, the quantum size-

effect for a 10 nm size is no more than 10 meV, even assuming infinite walls, and so this is not expected to be a significant factor in the room-temperature conduction.) We expect that there is disordered polymer at the grain boundaries that will contribute localized states forming much of the band tail that traps the carriers. Other papers have shown that the multiple-trapping formalism with a three-dimensional density of states provides a reasonable quantitative model for the transport in polycrystalline organic materials.[12–14]

We would like to estimate the mobility of free carriers in a lamella, and we can approach this from different limits. For example, theories of bandlike transport in amorphous, inorganic semiconductors suggest that the mobility at the mobility edge is of order 10 cm^2/Vs.[36] This value is obtained by considering that the minimum scattering length is of order 1 bond length and is also about the value obtained from measurements in amorphous silicon. This approach may set an approximate lower limit on band transport in the absence of a significant polaron effect.

In a perfect crystal, the mobility is determined by scattering from acoustic phonons. The mobility is proportional to the scattering length and is given by[37]

$$\mu = \frac{2.45\pi\hbar^4 Be}{\varepsilon_{ac}^2 (3kT)^{3/2} (m^*)^{5/2}}, \tag{5}$$

where B is the bulk modulus, ε_{ac} is the deformation potential, and m^* is the effective mass. The first principles calculations of the electronic structure in Sec. III give information about each of these parameters. The total energy of the polythiophene sheets was calculated as a function of interchain distance and the energy was fitted with a simple quadratic function, $\Delta E = K\Delta x^2$, to obtain $K = 0.70$ eV/Å^2 (for a single unit cell). For a deformation along the b axis (perpendicular to the chains),

$$B = V\frac{d^2E}{dV^2} = \frac{b}{ac}\frac{d^2E}{db^2} = \frac{b}{ac}(2K)$$

This yields $B = 3.8\times10^{-2}$ eV/Å$^3 = 6.1$ GPa, where a and b are given by the calculations and c is measured by x-ray diffraction ($\sim$1.8 nm). The deformation potential, defined as the energy shift of the valence band per unit change in the interchain spacing, is calculated to be approximately 2.7 eV. The same calculations also give effective masses (m^*/m) for the directions parallel and perpendicular to the polymer chains; these are 0.15 and 1.75 (for the holes) and 0.17 and 5.25 (for the electrons). Using these values to estimate the hole mobility, we obtain $\mu_{perp.} = 11$ cm^2/V s and $\mu_{parallel} = 4800$ cm^2/V s, and the respective mean free paths are 1.1 and 150 nm.

The large value estimated for the parallel mobility cannot be achieved in the nanocrystals, because the mean free path greatly exceeds the size of the nanocrystals. If there is scattering only at the boundary of a 10 nm lamella, the mobility can be no more than $\mu_{parallel} \sim 300-450$ cm^2/V s. However, there are two reasons to expect the mobility to be even smaller. First is the internal disorder of the lamella arising from small rotations and other distortions of the chains.[38] An inspection of the structure in Fig. 4 shows that rings can rotate easily, with respect to their neighbors, by thermal energy, and those rings with alkyl chains attached can be pulled out of alignment by disorder in the side-chain configurations. These effects reduce the conjugation length and the associated scattering length and mobility. However, we do not have a quantitative estimate for the increased scattering. The second effect to reduce the mobility arises from polarons. Even though the polaron effects are smaller in the ordered lamella than in the amorphous polymers, we do not doubt that they increase the effective mass and reduce the mobility compared to the calculations that do not include electron-phonon interactions. Again, further calculations are needed to quantify the magnitude of the effect.

In any event, the apparent mobility of the ensemble of lamella is an average of the values in the two directions, which tends to be dominated by the smaller mobility (see Sec. V). These estimates suggest that a polythiophene lamella has an effective hole mobility of order 10 cm^2/V s with an upper limit that is below 30 cm^2/V s. The electron mobility should be smaller because of the weaker π-π coupling, as indicated in Fig. 8.

Measurements of single-crystal organic small molecules usually find room-temperature mobility in the range of 1–30 cm^2/V s,[6,39] compared to 100–10 000 for inorganic covalent semiconductors. The lower values arise in part from the larger effective masses, because the bands are narrow, but mostly from the smaller elastic modulus typical of organic materials due to the Van der Waals bonding between molecules. According to Eq. (5), the mobility is proportional to the elastic modulus, so it seems highly unlikely that any organic semiconductors can have a high room-temperature mobility on the scale of the much harder, inorganic semiconductors.

B. Intergranular transport

The combined DOS of both ordered and disordered regions determines the transport. A key point that emerges, as illustrated in Fig. 10, is that states that are deep traps for the disordered regions now become shallower traps for the ordered regions, and many of the traps in the amorphous material are inaccessible as they lie within the valence band of the ordered material.

According to this picture, the grain boundaries are relatively empty of localized states above the valence band of the lamella. We consider alternative mechanisms of transport from grain to grain, based on the structural model.

1. Conduction along bridging polymer chains

Where there are polymer chains connecting the adjacent lamella, particularly those with small bend angles, we expect that transport across the grain boundary is relatively easy, with moderate energy traps from the disorder.

2. Tunneling or thermal activation

Where there is no low-angle grain boundary connecting the lamella, transport is less probable, because holes must tunnel across the barrier or fall into deep traps. At low temperature tunneling is the only available mechanism, but at

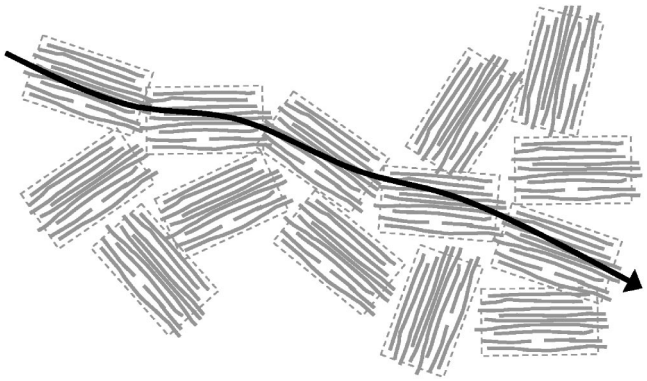

FIG. 12. Schematic illustration of the proposed transport path along preferential directions with low-angle grain boundaries, forming a high-mobility percolation path.

elevated temperatures there can be thermal activation through higher energy states of the disordered region.

Our conclusion is that intergranular transport is probably directional, favoring transfer between lamella of approximately the same orientation, at least at low temperature.

C. Dimensionality and percolation

The anisotropic nature of the polymer structure and conductance leads to the consideration of percolation effects in the transport, and this has been featured in a number of transport models for polymers.[40,41] The dimensionality of the transport process is important, and here there is a distinction between small-scale and large-scale dimensionality. In the case of an amorphous polymer, the dominant transport direction is along the polymer chains, so the material is locally one-dimensional. However, a disordered polymer has no preferred large-scale direction for the chains, so the long-range transport is three-dimensional; hence an isotropic transport model is appropriate.

In contrast, TFT transport in the plane of the ordered PAT lamella is two-dimensional under the assumption that the holes are delocalized and the scattering length is smaller than the nanocrystal size. The dimensionality of long-range transport depends on the transport between lamella. The previous discussion of the grain boundary suggests that there is a preferred direction for grain-to-grain transport, which occurs between grains with small angle differences. This suggests a one-dimensional transport process, as illustrated in Fig. 12. However, if the barrier for transport between grains with high-angle boundaries becomes small enough, for example, by thermal activation at sufficiently high temperature, then there will be a transition to two-dimensional transport. We expect that vertical transport perpendicular to the lamella will be more limited than transport in the plane, and, indeed, measurements of regioregular P3HT find a mobility of 3×10^{-4} cm^2/V s for vertical transport, which is $300\times$ smaller than the in-plane mobility.[42]

Low-dimensionality transport suggests an important role for percolation. The classic percolation system has locally conducting and insulating regions with bulk conduction only occurring when there is a complete conduction path. Here the situation is less well defined, in which the insulating regions have lower but nonzero conductance. An essential point about percolation is that it applies to a two-phase material, in this case high-mobility lamella and low-mobility disordered material. The percolation effects are such that the relative contributions of the two phases to the transport may be substantially different from their relative contributions to the volume of material. The possible effects of percolation are discussed below.

V. TRANSPORT MODEL CALCULATIONS AND COMPARISON WITH EXPERIMENT

Now we apply the analysis of the structure and electronic transport to a simple numerical model for transport in polythiophene. Since we lack accurate values for many parameters, the primary aim of the model is to see if reasonable estimates for the values yield an approximate fit to the data.

A. The mobility prefactor

First we discuss the mobility prefactor, as defined in Eq. (1). The transport data in Fig. 3 show an effective mobility that increases rapidly with temperatures between 250 and 400 K with an activation energy of about 0.23 eV and a mobility prefactor of $\sim$500 cm^2/V s, which greatly exceeds our estimates of the likely band mobility. In a model of bandlike transport and localized band-tail states, μ_{EFF} is determined by the fraction of carriers that are mobile,

$$\mu_{EFF} = \frac{1}{n_T}\int N(E)\mu(E)f(E,V_G,T)dE$$
$$\approx \frac{\mu_0}{n_T}\int_0^\infty N_V(E)\exp\left(-\frac{[E+E_F(T)]}{kT}\right)dE$$
$$= \frac{\mu_0 N_V kT}{n_T}\exp(-E_F(T)/kT), \quad (6)$$

where n_T is the total carrier density, and N_V is the density of states in the band, which starts at $E=0$. The approximations assume a constant mobility, constant DOS (because it is two-dimensional), and a Boltzmann distribution (though the Fermi distribution is used in the numerical calculations). The Fermi energy, E_F, generally increases with temperature (i.e., it moves further from the band edge). This is referred to as the statistical shift and is a factor in the temperature dependence of μ_{EFF}. Applying a linear approximation to the temperature dependence, $E_F = E_{F0} + \gamma_T T$, gives

$$\mu_{EFF} = \frac{\mu_0 N_V kT}{n_T}\exp(-\gamma_T/k)\exp(-E_{F0}/kT)$$
$$\equiv \mu_{PRE}\exp(-E_{F0}/kT). \quad (7)$$

The mobility prefactor μ_{PRE} is defined by Eq. (7) and determined by the various parameters. Localized band-tail states tend to make γ_T small; hence, $\mu_{PRE} \gg \mu_0$ when $N_V kT/n_T \gg 1$. The 2D density of states favors a large $N_V kT/n_T$, because the DOS increases abruptly at the band edge. A large

prefactor exceeding the actual band mobility is therefore not unexpected.

B. Numerical model for transport

Model calculations of the TFT transport are performed, guided by the above discussion. The features of the model are the following:

(a) A two-dimensional density of states is used for the ordered lamella, along with the assumption that transport is confined to a single plane of the lamella. The 2D DOS obtained from the band structure is about 2×10^{14} cm^{-2} eV^{-1} but, as discussed in Sec. IV A we think that neglect of disorder and polaron effects in the calculation of the perfect crystal overestimates the bandwidth, just as it overestimates the mobility. Hence, we compare model results for the calculated value of 2×10^{14} cm^{-2} eV^{-1}, as well as a larger DOS of 5×10^{14} cm^{-2} eV^{-1}.

(b) An exponential band tail of localized states is assumed, representing the disordered regions between the ordered grains, so that the combined DOS is as illustrated in Fig. 11. The band-tail density of states' slope and concentration are parameters of the model, but a reasonable fit to the data can only be obtained if the number of deep localized states is consistent with the measured threshold voltage.

(c) A constant mobility is assumed in the ordered regions representing transport in the ordered lamella. We also introduce an exponential energy-dependent mobility in the band tail $[\mu=\mu_{B0}\exp(-(E-E_B)/E_0)]$, which we attribute to the conduction from the disordered intergranular regions. Both are assumed for convenience to be independent of temperature, only because we lack any knowledge of their temperature dependence. The mobility in the band tail is certainly expected to be temperature dependent from a hopping mechanism. The energy-dependent band-tail mobility is based on the expectation that the transport in disordered regions will have a mobility that decreases rapidly as the DOS decreases; hence, we choose an exponential.

(d) Percolation effects are ignored in these calculations, but are discussed later.

The assumption of two-dimensional transport simplifies the calculation, since there is no requirement to calculate the potential profile into the semiconductor. The charge in the TFT channel is obtained from the gate capacitance (taken to be 3×10^{-8} F/cm^2, as used in the measurements).

Figure 13 shows the result of a calculation of $\mu_{EFF}(T)$ based on Eq. (6) and for two values of gate voltage (20 and 30 V). These calculations assume zero mobility in the localized states and are intended only to model the high-temperature region. The parameters were chosen first to ensure that the room-temperature mobility is about 0.1 cm^2/V s, as indicated by experiment, and then to reproduce the approximate temperature dependence and prefactor. The mobility and band-tail slope are 30 cm^2/V s and 0.1 eV for the lower DOS and 10 cm^2/V s and 0.08 eV for the higher DOS.

The mobility prefactor is 100–200 cm^2/V s for the different data sets, which is 1 order of magnitude larger than the band mobility and shows that $N_V kT/n_T$ is ~10 for a reasonable DOS. Hence the large, measured prefactor is consistent with the lower expected band mobility. The calculated activation energy is 0.175 and 0.20 eV for the different gate voltages and the larger DOS, which is somewhat smaller than the measured energy. The 300 K Fermi energy is 0.179 and 0.212 eV, respectively, showing that the statistical shift is indeed small. The calculations show that if the DOS is larger, then the prefactor is indeed larger, as expected from Eq. (7).

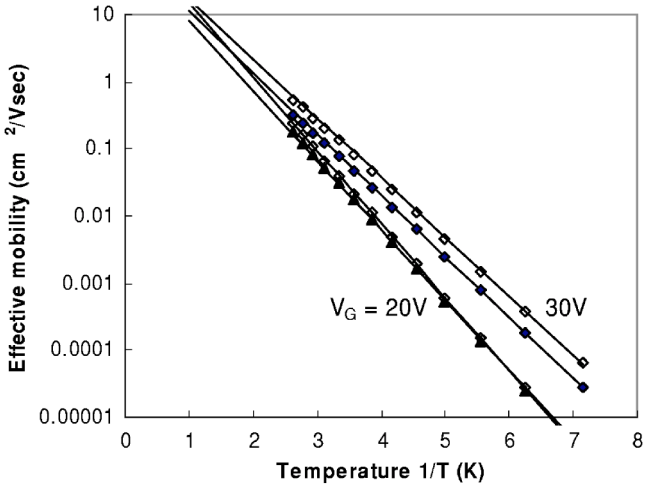

FIG. 13. Numerical calculation of the effective mobility in the high-temperature regime for two gate voltages, based on the model described in the text. The assumed DOS above the band edge is 2×10^{14} cm^{-2} eV^{-1} (open points) and 5×10^{14} cm^{-2} eV^{-1} (closed points), the band mobility is 30 and 10 cm^2/V s respectively, and the other parameters are given in the text.

The difference between the 20 and 30 V mobility values implies a significant threshold voltage; otherwise the results would be identical. We find that although the model is in reasonable agreement with the data, obtaining an exact fit is difficult. The reason is that a large mobility prefactor is obtained when there is a large density of localized states to pin the Fermi energy, but then there is also a large threshold voltage. We have not explored all parameters fully to find the best fit, but we suspect that there is still an additional aspect of the transport, as discussed below.

The Fermi energy changes only slowly with temperature, so that the measured activation energy reflects the position of the Fermi energy with respect to the conductivity energy, apart from the statistical shift, which, as discussed above, we think must be relatively small. The smaller mobility activation energy at low temperature then suggests a different transport path at lower energy. Hence, we model this behavior by including the energy-dependent mobility in the band tail.

Figure 14 shows the results of the same calculation of effective mobility as in Fig. 13, with the addition of the nonzero band-tail mobility. At low temperature the mobility activation energy decreases and eventually becomes independent of temperature. This corresponds to transport in the band tail, at the Fermi energy, but in a more realistic model we expect a temperature dependence. The temperature at which the change of slope occurs depends on the choice of

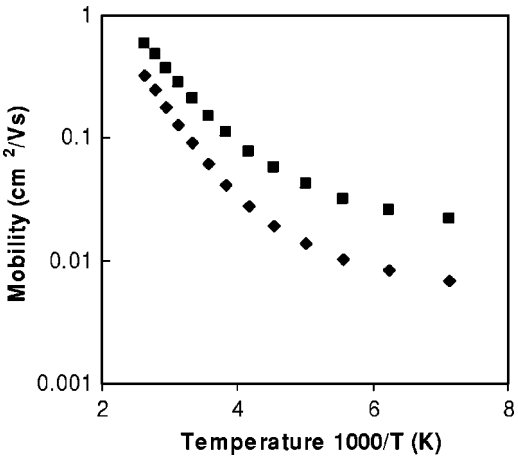

FIG. 14. Numerical calculation of the effective mobility, with the same parameters as for Fig. 13, but including a nonzero band-tail mobility.

parameters for the energy dependence of the band-tail mobility and on the gate voltage. Reasonable parameters give a change of slope at the observed value of 250 K. We could easily obtain a better fit to the low-temperature region by making the reasonable assumption that the band-tail mobility is temperature dependent, but it does not seem useful to add more parameters at this level of development of the model. The data show that the gate-voltage dependence is largest at low temperature, which is consistent with the measured increase in the threshold voltage.

A separate numerical calculation of the TFT mobility, μ_{TFT}, is also performed. The TFT transfer characteristics in the linear regime are calculated as a function of gate voltage at different temperatures. The position of the Fermi energy at each gate voltage and temperature is obtained from the channel charge by an iterative calculation. We extract the TFT mobility by fitting the I_D-V_G calculation to a straight line

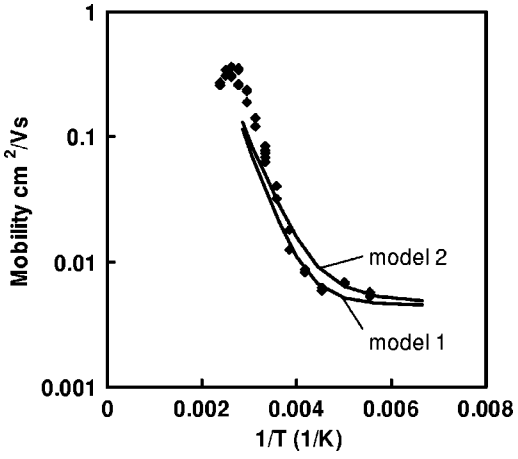

FIG. 15. Numerical calculation of the TFT mobility (lines) obtained by calculating the linear transfer characteristics, compared to the measured data (points). The model includes a nonzero band-tail mobility. The DOS is 5×10^{14} cm^{-2} eV^{-1} for model 1 and 2×10^{14} cm^{-2} eV^{-1} for model *2*, with the other parameters chosen to give the best fit.

over a range of V_G. Figure 15 shows two examples of calculations of μ_{TFT} for DOS parameters equal to the calculated number and the larger values and with a band mobility of 50 and 40 cm^2/V s, respectively. Other parameters, such as $\mu(E)$ in the band tail, are varied to give a reasonable fit to the data. The main point is that the model is again able to reproduce the form of the experimental data, even including the threshold voltage. The change of slope at about 250 K again originates from the assumption of low-mobility carriers in the band tail, and, without this assumption, this form of the data could not be obtained. The temperature at which the slope change occurs and the magnitude of the current at the transition depends on the band-tail slope and the energy dependence of the mobility.

We are able to reproduce the large activation energy and prefactor for the high-temperature region, and this is related both to the assumed band mobility and the shape of the band tail. However, this model assumes a larger band mobility than the calculations in Fig. 13, to obtain a good fit. The reason is that the model does not allow a choice of threshold voltage, because this is taken out of the calculation. In order to get a good fit we need to assume a lower density of band-tail states, and the statistical shift of E_F then plays a larger role. We therefore again find that it is difficult to find an acceptable set of parameters that give the correct mobility and threshold voltage. We suggest that percolation may be the missing aspect of the model, and this is discussed next.

C. Percolation and mixtures

We can only estimate the role of percolation qualitatively. We consider a material which has a high mobility, μ_H, operating in a portion of the volume, V_H, and a low mobility, μ_L, operating in volume, V_L. If carriers randomly pass through both materials, then the mobility of the mixture, μ_{MIX}, is given by

$$\mu_{MIX} = V\mu_H\mu_L/[\mu_H V_L + \mu_L V_H]. \tag{8}$$

When $\mu_H/\mu_L \gg 1$, then $\mu_{MIX} \sim \mu_L\ V/V_L$, unless V_L is sufficiently small that $V_L/V \ll \mu_L/\mu_H$. Hence, the mobility of a mixture is typically controlled by the smaller mobility value. In this sense, it is perhaps surprising that PQT-12 with small nanocrystals and significant disordered material in the grain boundaries has the high mobility that is measured. Part of the explanation is the shift of the band edge in the ordered material, and another reason is attributable to percolation.

Percolation changes the analysis by considering the different paths through the material. For each conduction path through the material, there is a mobility corresponding to the values of V_H and V_L for the path. Assuming $V_L = fV$, then from Eq. (8),

$$\mu_{path} \sim \mu_H/[1 + f\mu_H/\mu_L]. \tag{9}$$

The percolation approach recognizes that there are many parallel conduction paths with different values of f, and the overall conduction is dominated by the few paths with the highest mobility, in which f is small and $\mu_{path} \sim \mu_H$. Instead of mobilities that add in series, for which the lower value dominates, the mobilities of different paths add in parallel, and the larger value dominates.

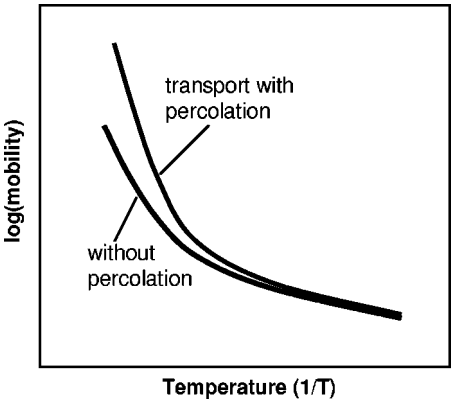

FIG. 16. Schematic diagram showing the increase in the temperature dependence of the mobility when percolation is taken into account.

The point of this discussion is that percolation may also modify the temperature dependence of the TFT conductivity, because the percolation paths change with temperature. At low temperature, the disordered regions provide a high degree of isolation between ordered regions, and there may be only a few high-mobility percolation paths. As the temperature increases, enhanced conduction in disordered regions provides conduction between more lamella, creating more percolation paths, and at high-enough temperature the barriers between lamella do not significantly limit transport. The transport paths interconnect, and many more percolation paths are effective. We therefore expect that the conductivity increases with temperature faster than is expected from an isotropic 2D conduction model, and the mobility is as illustrated in Fig. 16.

In summary, although we cannot provide a quantitative model, we suggest that percolation has a significant role in the transport. It is hard to estimate the magnitude of the effect, but an additional increase in conduction by a factor ~ 2 between 250 and 400 K, would be enough to greatly improve the fit of the numerical model to the data.

VI. DISCUSSION

Additional information is needed to make the model more quantitative and to extract reliable parameters. For example, more detail about the degree of disorder within the lamella crystal structure and in the grain boundaries would improve estimates of the electronic structure, and calculations of scattering from disorder within crystallites would improve the estimate of the mobility. Independent measurements of the DOS would be valuable. The quantitative role of percolation is also not known in detail.

Large crystal size is obviously helpful in reducing the fraction of disordered material at the grain boundaries. However, a crystal size of order 10 nm seems to form a natural limit in a wide range of polymers. Kline *et al.* show an increase in mobility of P3HT with molecular weight (MW) up to about 30 kD, which is associated with a change in crystal ordering visible in AFM.[25] However, the crystallinity is in fact higher in the low-MW materials than in the high-MW materials. Kline *et al.* suggest that the effect must be due to the grain boundaries which are sharper for the low-MW material as seen by AFM.

Percolation could explain why some measurements of transport in polythiophenes find an increase in the mobility with an alignment layer and some measurements do not. Heil *et al.* report a factor 8 increase in TFT mobility using a rubbed alignment layer,[27] but the mobility is rather low ($\sim 10^{-4}$ $\mathrm{cm}^2/\mathrm{V\,s}$) and Sirringhaus *et al.* report a similar alignment effect in polyfluorene.[26] The alignment of crystallites should create more low-angle grain boundaries and therefore increase the number of percolation paths. The largest effect is expected when the mobility is otherwise low. The mobility should be less sensitive to increased alignment when there are already many high-mobility percolation paths.

According to our analysis, the ordering of the polymer structure has two effects. First, the volume of amorphous material is decreased, so their associated localized-state density is reduced. Hence, even if the transport remains dominated by hopping in the disordered material, the conductivity will increase because the Fermi energy moves further up the DOS for a given gate voltage, and the exponential increase in hopping conductivity more than offsets the reduced volume of material. The second effect is that the lamella provide a higher mobility transport path that is accessible to holes. We therefore anticipate different regimes of conduction, as follows:

(a) A fully amorphous material. Isotropic conduction (at a larger-length scale than the polymer chain) is dominated by hopping, exhibiting a low mobility and a high effective activation energy (or $T^{1/n}$ hopping, where n depends on the dimensionality).

(b) A mixture of amorphous and ordered material in which the amorphous material forms the dominant percolation path. Conduction is primarily through the amorphous regions. The ordered regions remove states and enhance the conduction, compared to fully amorphous material. Transport in the amorphous regions is favored at low temperature.

(c) A mixture of ordered and amorphous materials, with the ordered material forming the dominant percolation path. The higher mobility of the ordered material dominates the conduction, and high temperatures favor this mechanism. As the fraction of disordered material decreases, the Fermi energy moves closer to the band edge, so that both the ordered and disordered regions are more conducting at a specific gate voltage. The transport model described here applies to this situation.

Finally, it is also interesting to compare the crystallinity and transport in different organic semiconductors. For example, pentacene has a polycrystalline structure, and the TFT mobility depends on the crystal size, which can be changed by varying the deposition temperature. The mobility of pentacene is about 1 $\mathrm{cm}^2/\mathrm{V\,s}$ when the grain size is ~ 1 μm or more, and it is within a factor ~ 3 of the single crystal mobility. However, a grain size of ~ 100 nm (typically obtained by lowering the deposition temperature) reduces the mobility by 2–3 orders of magnitude.[43] By comparison, a grain size as small as 10–20 nm gives high mobility in polythiophene. Apparently, relative to pentacene, the grain boundaries in PAT do not limit the mobility as much as in pentacene, even

though highly disordered PAT itself has very low mobility. The hole delocalization property may account for this result.

VII. CONCLUSIONS

We have tried to develop the elements of a transport model that accounts for the physical and electronic structures of ordered PATs, and which is perhaps extendable to other ordered polymers. Although many details are not known precisely, the model gives a good qualitative representation of the transport and at least semiquantitative agreement. The model is able to reproduce the change in slope of the mobility of PQT-12 near 250 K, by assuming low-mobility states within the band-tail distribution. This may be a good indication that there are two transport processes in operation, which is consistent with the proposed structural model of ordered lamella and disordered intergranular material. The model also helps to put limits on the value of the microscopic mobility in lamella and on what needs to be known to extract an improved value from the TFT data. The results of the model are consistent with a free mobility of about 10 $cm^2/V\,s$, which is in line with theoretical expectations. However, given the many uncertainties, accurate parameters cannot yet be extracted.

ACKNOWLEDGMENTS

The authors thank A. Arias, M. Chabinyc, and B. Ong for helpful discussions, the Xerox Research Center of Canada (B. S. Ong and Y. Wu) for providing the PQT-12 material, and the PARC process line for assistance in sample preparation. This work is partially supported by the Advanced Technology Program of the National Institute of Standards and Technology (Contract No. 70NANB0H3033).

*Email address: street@parc.com

[1] A. Tsumura, H. Koezuka, and T. Ando, Appl. Phys. Lett. **49**, 1210 (1986); Z. Bao, A. Dodabalapur, and A. J. Lovinger, *ibid.* **69**, 4108 (1996).

[2] G. Horowitz, M. E. Hajlaoui, and R. Hajlaoui, J. Appl. Phys. **87**, 4456 (2000).

[3] H. Sirringhaus, P. J. Brown, R. H. Friend, M. M. Nielsen, K. Bechgaard, B. M. W. Lanveld-Voss, A. J. H. Spiering, R. A. J. Jannsen, E. W. Meijer, P. Herwig, and D. M. de Leeuw, Nature (London) **401**, 685 (1999).

[4] G. Wang, J. Swensen, D. Moses, and A. J. Heeger, J. Appl. Phys. **93**, 6137 (2003).

[5] B. S. Ong, Y. Wu, P. Liu, and S. Gardner, J. Am. Chem. Soc. **126**, 3378 (2004); B. S. Ong, Y. Wu, P. Liu, S. L. Jiang, and K. Murti, Synth. Met.. **142**, 49 (2004).

[6] N. Karl, K-H. Kraft, J. Marktanner, M. Munch, F. Schatz, R. Stehle, and H-M. Uhde, J. Vac. Sci. Technol. A **17**, 2318 (1999).

[7] H. Bässler, Philos. Mag. B **50**, 347 (1984); H. Bässler, Phys. Status Solidi B **175**, 15 (1993).

[8] V. I. Arkhipov, P. Heremans, E. V. Emelianova, G. J. Adriaenssens, and H. Bässler, Appl. Phys. Lett. **82**, 3245 (2003); R. V. Rakhmanova and E. M. Conwell, *ibid.* **76**, 3822 (2000).

[9] M. C. J. M. Vissenberg and M. Matters, Phys. Rev. B **57**, 12 964 (1998).

[10] R. D. McCulloch and P. C. Ewbank, *Handbook of Conducting Polymers*, edited by T. A. Skotheim, R. L. Elsenbaumer, and J. R. Reynolds, (Marcel Dekker, New York, 1998), chap. 9 and references therein.

[11] H. E. A. Huitema, G. H. Gelinck, J. B. P. H. Van der Putten, K. E. Kuijk, K. M. Hart, E. Cantatore, and D. M. De Leeuw, Adv. Mater. (Weinheim, Ger.) **14**, 1201 (2002).

[12] G. Horowitz, R. Hajlaoui, and P. Delannoy, J. Phys. III **5**, 355 (1995).

[13] A. R. Volkel, R. A. Street, and D. Knipp, Phys. Rev. B **66**, 195336 (2002).

[14] A. Salleo, T. W. Chen, A. R. Volkel, Y. Wu, P. Liu, B. S. Ong, and R. A. Street, Phys. Rev. B **70**, 115311 (2004).

[15] T. Li, P. P. Ruden, I. H. Campbell, and D. L. Smith, in *Two-Dimensional Modeling of Organic Field-Effect-Transistors*, edited by Ghassan E. Jabbour, Sue Anne Carter, Junji Kido, Shuit-Tong Lee, and Niyazi Serdar Sariciftci, Mater. Res. Soc. Symp. Proc. No. 725 (Materials Research Society, Warrendale, PA, 2002), p. P10.2.

[16] A. K. Kapoor, S. C. Jain, J. Poortmans, V. Kumar, and R. Mertens, J. Appl. Phys. **92**, 3835 (2002).

[17] H. Sirringhaus, N. Tessler, and R. H. Friend, Science **280**, 1741 (1998).

[18] T. Muck, M. Leufgren, A. Lebib, T. Borzenko, J. Geurts, G. Schmidt, L. W. Molenkamp, V. Wagner, and H. L. Gomes, in *Electrical Characterization of Vacuum Deposited and Solution Processed DH4T Thin Film Transistors*, edited by P. W. Blom, N. C. Greenham, C. D. Dimitrakopoulos, and C. D. Frsibie, Mater. Res. Soc. Symp. Proc. No. 771 (Materials Research Society, Warrendale, PA, 2003), p. L10.31.

[19] E. J. Meijer, D. B. A. Rep, D. M. de Leeuw, M. Matters, P. T. Herwig, and T. M. Klapwijk, Synth. Met. **121**, 1351 (2001).

[20] A. Arias, S. E. Ready, R. Lujan, W. S. Wong, K. E. Paul, A. Salleo, M. Chabinyc, R. Apte, R. A. Street, Y. Wu, P. Liu, and B. S. Ong, Appl. Phys. Lett. **85**, 3304 (2004); A. Salleo and R. A. Street, J. Appl. Phys. **94**, 471 (2003); A. Salleo and R. A. Street, Phys. Rev. B **70**. 235324 (2004); M. Chabinyc, J.-P. Lu, R. A. Street, Y. Wu, P. Liu, and B. S. Ong, J. Appl. Phys. **96**, 2063 (2004).

[21] A. Salleo, M. L. Chabinyc, M. S. Yang, and R. A. Street, Appl. Phys. Lett. **81** (23), 4383 (2002).

[22] M. Chabinyc, A. Salleo, Y. Wu, B. S. Ong, M. Heeney, and I. M. McCulloch, J. Am. Chem. Soc. **126**, 13 928 (2004),

[23] N. Zhao, G. A. Botton, S. Zhu, A. Duft, B. S. Ong, Y. Wu, and P. Liu, Macromolecules **37**, 8307 (2004).

[24] B. Grevin, P. Rannou, R. Payerne, A. Pron, and J.-P. Travers, Adv. Mater. (Weinheim, Ger.) **15**, 881 (2003).

[25] R. J. Kline, M. D. McGehee, E. N. Kadnaikova, J. Liu, and M. J. Frechet, Adv. Mater. (Weinheim, Ger.) **15**, 1519 (2003).

[26] H. Sirringhaus, R. J. Wilson, R. H. Friend, M. Inbasekaran, W. Wu, E. P. Woo, M. Grell, and D. D. C. Bradley, Appl. Phys. Lett. **77**, 406 (2000).

[27] H. Heil, T. Finnberg, N. Von Malm, R. Schmechtel, and H. Von Seggern, J. Appl. Phys. **93**, 1636 (2003).
[28] R. Stumpf and M. Scheffler, Comput. Phys. Commun. **79**, 447 (1994).
[29] N. Troullier and J. L. Martins, Phys. Rev. B **43**, 1993 (1991).
[30] W. Kohn and L. J. Sham, Phys. Rev. **140**, 1133 (1965); D. M. Ceperley and B. J. Alder, Phys. Rev. Lett. **45**, 566 (1980).
[31] J. E. Northrup, M. L. Tiago, and S. G. Louie, Phys. Rev. B **66**, 121404 (2002); J. E. Northrup and M. L. Chabinyc, Phys. Rev. B **68**, 041202 (2003).
[32] M. L. Tiago, J. E. Northrup, and S. G. Louie, Phys. Rev. B **67**, 115212 (2003).
[33] P. J. Brown, D. S. Thomas, A. Kohler, J. S. Wilson, J.-S. Kim, C. M. Ramsdale, H. Sirringhaus, and R. H. Friend, Phys. Rev. B **67**, 064203 (2003).
[34] X. M. Jiang, R. Osterbacka, O. Korovyanko, C. P. An, B. Horovitz, R. A. J. Janssen, and Z. V. Vardeny, Adv. Funct. Mater. **12**, 587 (2002).
[35] M. Wohlgenannt, X. M. Jiang, and Z. V. Vardeny, Phys. Rev. B **69**, 241204 (2004).
[36] N. F. Mott and E. A. Davis, in *Electronic Processes in Noncrystalline Materials* (Clarendon Press, Oxford, 1979).
[37] N. Karl in *Organic Electronic Materials*, edited by R. Farchioni and G. Grosso (Springer, Berlin, 2001), p. 289.
[38] Z. G. Yu, D. L. Smith, A. Saxena, R. L. Martin, and A. R. Bishop, Phys. Rev. Lett. **84**, 721 (2000).
[39] V. C. Sundar, J. Zaumseil, V. Podzorov, E. Menard, R. L. Willett, T. Someya, M. E. Gershenson, and J. A. Rogers, Science **303**, 1644 (2004).
[40] A. N. Samukhin, V. N. Prigodin, and L. Jastrabik, Phys. Rev. Lett. **78**, 326 (1997).
[41] O. Levy and D. Stroud, J. Phys.: Condens. Matter **9**, L599 (1997); M. Reghu, C. O. Yoon, C. Y. Yang, D. Moses, Paul Smith, A. J. Heeger, and Y. Cao, Phys. Rev. B **50**, 13 931 (1994).
[42] K. Kaneto, K. Hatae, S. Nagamatsu, W. Takashima, S. S. Pandey, K. Endo, and M. Rikukawa, Jpn. J. Appl. Phys., Part 1 **38**, 1188 (1999).
[43] D. Knipp, R. A. Street, and A. R. Völkel, Appl. Phys. Lett. **82**, 3907 (2003).